THE JOURNAL OF PHYSICAL CHEMISTRY C

Article

pubs.acs.org/JPCC

Thin Film Approach to Single Crystalline Electrochemistry

Joshua Snyder, Nemanja Danilovic, Arvydas P. Paulikas, Dusan Tripkovic, Dusan Strmcnik, Nenad M. Markovic, and Vojislav R. Stamenkovic*

Materials Science Division, Argonne National Laboratory, Argonne, IL 60439, United States

ABSTRACT: Implementation of single-crystal metal electrodes into standard electrochemical procedures has provided invaluable insight into the structure of and processes occurring at the metal−electrolyte interface. However, the accuracy required in their manufacture to provide ideally cut crystals with the lowest possible degree of miscut in conjunction with the amount of material required, especially in the case of precious metals, can make their use highly restrictive. We present here fundamental insight into a general procedure for producing thin metal films containing large, atomically flat (111) terraces without the use of an epitaxial template. Thermal annealing in a controlled atmosphere induces long-range ordering in magnetron sputtered thin metal films deposited on an amorphous substrate. The ordering transition in these thin metal films yields characteristic (111) electrochemical signatures with minimal amount of material and provides an adequate replacement for oriented bulk single crystals. Moreover, this approach can be generalized and applied toward development of a new class of thin-film-based catalysts.

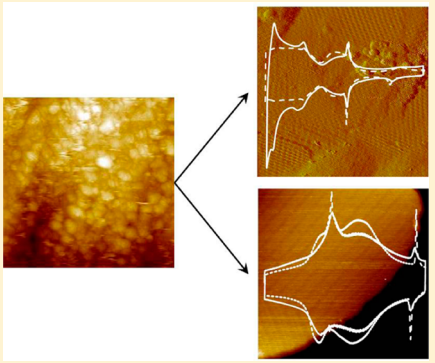

1. INTRODUCTION

Single-crystal metal electrodes hold a special place in the historical evolution of the field of surface electrochemistry, helping to shape fundamental understanding of the structure−function relationship and processes occurring at the metal−electrolyte interface. The use of single crystals and their stepped and vicinal families has aided the quest to deconvolute the activity contributions of surface structure such as terraces, steps, and kinks and overall crystallographic orientation from electronic effects. The investigation of the mechanistic reaction pathways relevant to the hydrogen economy has also been greatly facilitated by single crystals, most prominently the oxygen reduction reaction (ORR),[1−4] providing valuable insight into the link between bulk surfaces and nanoscale catalysts.[5−7] In this vain, Pt(111)[8] has been the model single crystal as its close-packed surface and wide atomically flat terraces provide an ideal reaction surface essentially devoid of defects when properly prepared. Extension of the methodology to oriented crystals of single-phase metal alloys has inspired and guided a whole branch of electrocatalyst research and development focused on optimization of catalyst interaction with reaction intermediates and products. Most notably, the discovery that a unique compositional profile developed through annealing of a $Pt_3Ni(111)$ single crystal where a Pt skin covering a Ni- rich second atomic layer was found to be the most active surface to date for the ORR.[9]

Routine utilization of single crystals was made ubiquitous by J. Clavilier et al.[10−12] through introduction of a technique to reproducibly prepare single-crystal bead electrodes by melting and carefully cooling metal wires followed by X-ray orientation, cutting, and polishing to expose the desired crystallographic face. However, proper orientation and cutting of the crystal is a challenging process where even small degrees of miscut can result in significantly altered structural and electrochemical properties.[13−16] While useful for determining the electrochemical signature and for chronocoulometric and amperometric studies, small bead-type electrodes are not ideal for kinetic investigations requiring the use of a rotating disk electrode (RDE). The cylindrical single-crystal geometry is more amenable to the RDE where the electrodes are typically several millimeters in diameter and thickness, requiring a significant amount of material. Moreover, they can only be manufactured in a limited number of facilities that have the capabilities to grow, orient, cut and polish bulk single crystalline rods. Consequently, cylindrical, bulk single crystals are cost-prohibitive for general use, especially considering that most electrocatalysts are based on precious metals such as Pt and Au. The thin-film approach offers an intriguing alternative as the nature of their geometry makes them susceptible to ordering upon controlled heat-treatment, driven by a tendency to expose the lowest energy surface, (111) family. Promotion of (111) orientation for thin films is typically achieved through epitaxial growth on single-crystal metal, metal oxide, glass or mica substrates either by slow vapor phase growth such as evaporative[15,17−21] and physical vapor deposition (PVD)[22−24] or in solution through electrochemical deposition.[25,26] While films produced in this manner have low roughness factors and strong (111) texture as evidenced by X-ray diffraction (XRD), they can be highly strained because of the lattice mismatch between the film and the substrate and are typically plagued with holes or discontinuities evolved during annealing as a result of film dewetting from the substrate. As a consequence,

Received: August 5, 2013
Revised: September 20, 2013
Published: October 1, 2013

   dx.doi.org/10.1021/jp4078272 | J. Phys. Chem. C 2013, 117, 23790−23796

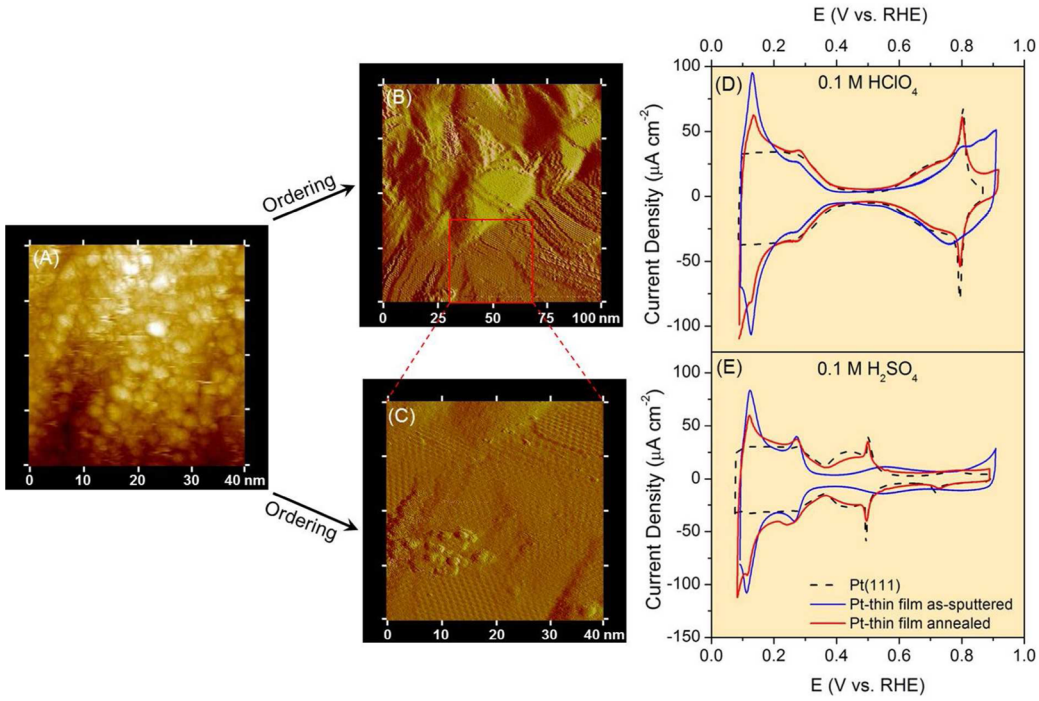

Figure 1. Scanning tunneling microscopy (STM) images of (A) as-sputtered Pt thin film and (B,C) a CO_{ad} layer on annealed Pt thin film on a GC substrate. The hexagonal structures shown in (B) and (C) are attributed to an ordered CO_{ad} layer that is visible only on clean, atomically flat (111) terraces. From this image it is clear that the annealed Pt thin film is composed of a local structure containing terraces of width greater than 20 nm. Cyclic voltammograms of Pt(111) (black dashed line), as-sputtered Pt thin film (blue line), and annealed Pt thin film (red line) in room temperature, Ar purged (D) 0.1 M $HClO_4$ and (E) 0.1 M H_2SO_4, recorded with a sweep rate of 50 mV s^{-1}.

they often lack the long-range order required to exhibit the cyclic voltammetric (CV) fingerprint adsorption features characteristic of (111) single crystals.[17,18,26,27] Pt thin films displaying a strong (111) texture and exhibiting the characteristic Pt(111) electrochemical signature in $HClO_4$ have been prepared through sputter deposition of Pt onto Si/SiO_2 substrates using a Ti buffer layer.[28,29] Flame annealing was used to drive ordering of the surface, resulting in clean voltammetry characteristic of Pt(111); however, through examination of their scanning electron microscopy (SEM) and scanning tunneling microscopy (STM) images, it is clear the films contain a significant fraction of holes, possibly due to dewetting during the heat treatment or melting of a film that was initial composed of large columnar grains separated by voids created during sputter deposition. Also, integration of these thin films into an RDE, while possible, can be difficult with thin Si wafer substrates resulting, for example, in ORR polarization curves lacking a clear delineation between the diffusion and mixed kinetic/diffusion limited regions.[29] Use of a SiO_2 layer could also add a resistive component to the electrode that may interfere with determination of kinetic parameters from electrochemical data.

In this report, we present a rapid and reproducible approach for generating thin metal films that exhibit strong (111) character without the use of epitaxial templates or seeded layer growth. Structural ordering of magnetron sputter-deposited thin films during low-temperature annealing in a controlled atmosphere driven by surface energy reduction yields an ordered (111) surface structure as evidenced both through their electrochemical signature and observation of (111) hexagonal features by STM. These (111)-like films are ideal for mechanistic investigations of electrochemical and charge-transfer processes, serve as templates for development of next generation, practical electrocatalysts, and provide insight into the link between extended, bulk surfaces and nanoscale systems.

2. EXPERIMENTAL SECTION

Thin films were prepared by magnetron sputter deposition onto glassy carbon (GC) disks (6 mm dia., 4 mm thick) in an ultra-high vacuum (UHV) sputter deposition chamber with a base pressure of 10^{-10} torr. Prior to deposition of metal films, GC substrates were cleaned with RF Ar plasma. Pt films were deposited at room temperature at a rate of 0.75 Å/s, while Au films were deposited at room temperature at a rate of 0.74 Å/s. Films of both Pt and Au were between 10 and 25 nm thick. As-deposited films were annealed for 2 h in a tube furnace under controlled atmosphere, 3% H_2/Ar, at 500 °C for Pt and 300 °C for Au.

A typical three-compartment, pyrex electrochemical cell was used for all electrochemical measurements where the saturated calomel electrode (SCE) (Hg/HgCl, Beckman) reference electrode was separated from the working electrode compartment by a salt bridge and the Pt counter electrode was separated with a porous glass frit. All potentials in this study are reported versus the reversible hydrogen electrode (RHE). Thin, sputtered or annealed films on GC disks were characterized electrochemically in the hanging meniscus configuration in Ar-purged 0.1 M $HClO_4$ and 0.1 M H_2SO_4 electrolytes which were made from high-purity acids. Thin films were immersed in the electrolyte under potential control (0.1 V versus RHE).

The scanning tunneling microscopy (STM) images for the Pt thin films were acquired with a Digital Instruments Multi-Mode Dimension STM controlled by a Nanoscope III control station. During the measurement, the microscope and sample were

dx.doi.org/10.1021/jp4078272 | J. Phys. Chem. C 2013, 117, 23790−23796

enclosed in a cylinder pressurized with a CO atmosphere at 115 kPa. Prior to introduction of the sample into the STM, a CO layer was adsorbed onto the surface in CO-saturated 0.1 M $HClO_4$ both to preserve the order and cleanliness of the surface and to aid in visualization of the surface atomic structure with respect to the formation of an ordered adlayer of CO.

STM images for the Au and Pt thin films were also recorded in an Omicron UHV system equipped with an STM chamber. Samples were imaged at +0.20 V and 1.0 nA.

3. RESULTS AND DISCUSSION

Magnetron sputter deposition is a versatile and efficient method to quickly grow thin single-component, layered, and well-mixed alloy films with the number of components limited only by the number and composition of targets within the sputter chamber. As-sputtered films, however, are characterized by an atomically rough, three-dimensional surface morphology with grain sizes averaging 5 nm (Figures 1A and 4A) and electrochemical properties characteristic of bulk polycrystalline materials (Figures 1 and 3). The electrochemically active surface area as determined by the charge associated with hydrogen underpotential deposition (H_{UPD}) for an as-sputtered Pt thin film (Figure 1D,E) is not much greater than the geometric surface area of the GC disk. This is important to emphasize as the GC disks themselves have a roughness factor considerably higher than that of a single-crystal epitaxial template or Si/mica wafers. Such an outcome is in agreement with fine-tuning of the sputter deposition parameters which have direct consequences on the ability of the film to form an ordered surface structure upon annealing. Moreover, we are aiming toward a film with a dense and compact structure, avoiding columnar grains with highly grooved grain boundaries extending to the underlying substrate. In that case, grain growth and ordering during annealing would be limited as grain boundaries impinged on the surface of the substrate may be resistant to movement and will consequently slow grain coalescence and growth, especially at moderate annealing temperatures. Through our approach, dense films are formed by using a low sputter gas pressure which limits the amount of process gas entrapped in the film and also allows the bombarding ions to maintain their kinetic energy, facilitating diffusion and rearrangement after impingement on the surface. The high kinetic energy of the sputtered ions imparts high mobility to the deposited atoms on the growing surface, producing a sputtered film, for FCC metals, with a predominately (111) orientation of individual grains.[30,31] However, the surface morphology of an as-sputtered film is atomically rough with small grains whose surface orientations are not necessarily (111), as seen in Figures 1A and 4A.

Annealing thin films in a reductive atmosphere facilitates surface diffusion, which tends to smoothen defects and promote growth of lowest energy (111) facets, leading to thin film surfaces dominated by large (111) domains. Use of an amorphous substrate and film thicknesses under 30 nm promotes rearrangement of the film morphology at moderate annealing temperatures as it is not epitaxially constrained to the crystallographic structure of the underlying substrate; hence, surface diffusion and grain boundary motion are sufficiently fast to induce coalescence and growth of grains. Care must be taken, however, when annealing thin, sputtered films as competitive atomic processes, smoothening driven by surface energy reduction and roughening through hillock and hole formation driven by film stress reduction, can result in discontinuous, rough films. For instance, films sputtered at low pressures, below a transition pressure characteristic to the particular metal, are typically in compression.[32−34] In these films, atomic motion during annealing can tend to relieve this stress by forming mounds or hillocks on the surface of the film. Consequently, for thin films, the metal around the base of these mounds can quickly deplete, creating holes extending to the underlying substrate.[35−37] In addition, film roughening during annealing can also occur through grain boundary grooving[38] as well as induction of stress by a difference in the thermal expansion coefficients between the metal film and the substrate, which tends to cause the film to dewet from the substrate.[39] These issues become more problematic as the film thickness and melting point of the metal decrease. We have found that film roughening can be avoided by using moderate annealing temperatures, $\sim 0.3\ T_m$ (melting point), above which film dewetting and carbon impurity incorporation from the GC substrate is evidenced by the loss of characteristic (111) features in the CV plots. These lower temperatures prove to be sufficient to induce surface diffusion-driven structural ordering in the thin films; slower, bulk diffusion is not required to reach the desired surface structure.

Figure 1D,E compares the CV plots of Pt(111), as-sputtered Pt thin film, and annealed Pt thin film in both $HClO_4$ and H_2SO_4. The as-sputtered Pt thin film has an electrochemical signature resembling that of a polycrystalline Pt electrode with H_{UPD} peaks associated with proton adsorption on step and defect sites and broad oxidation−reduction features at higher potentials, consistent with the film's small-grained, atomically rough surface. By annealing the films in a reductive atmosphere, surface diffusion driven by the tendency to revert to the lowest energy surface, the (111) face, results in the formation of a well-defined, long-range order. The surface of the film is transformed from an atomically rough, small-grained morphology to one that is well-ordered, characterized by large, interconnected, atomically flat terraces with widths greater than 20 nm as shown by the hexagonal (2×2)-3CO adstructure of the CO_{ad} layer on Pt in the STM images in Figure 1B,C; an adsorbate structure that occurs only on atomically flat (111) terraces.[40]

The CV plots of the annealed Pt thin film show characteristic features of Pt(111) in both $HClO_4$ and H_2SO_4 electrolytes, Figure 1D,E. In $HClO_4$, Figure 1D, one can see that the region of the curve attributed to H_{UPD}, 0.1 to 0.4 V versus RHE, flattens after annealing, moving toward a current that is independent of potential, which is characteristic of a nearly defect free surface. However, there are current peaks associated with hydrogen adsorption−desorption from (100) and (110) sites as the thin film retains some polycrystalline features. As the potential is swept anodically, a sharp, reversible butterfly feature appears at ∼0.8 V versus RHE for the Pt(111) electrode and annealed Pt thin film, a feature that is absent for the as-sputtered Pt thin film. This feature is attributed to adsorption−desorption of OH_{ad} species, and its peak current and sharpness is a descriptive metric for both the cleanliness and ordering of the surface as well as the cleanliness of the electrolyte solution.[41−44] The magnitude of the butterfly peak currents for the annealed Pt thin film are nearly equal to those of Pt(111), indicative of the long-range ordering associated with large, interconnected (111) terraces present on the annealed thin film (Figure 1B). This ordering is further confirmed in 0.1 M H_2SO_4 electrolyte (Figure 1E), where a butterfly peak appears at ∼0.5 V versus RHE; the position is dependent upon

dx.doi.org/10.1021/jp4078272 | J. Phys. Chem. C 2013, 117, 23790−23796

HSO_4^- concentration in solution.[13,45] This reversible feature has been attributed to the order−disorder transition of an adsorbed sulfate adlayer, and the sharpness of the peak is due to a sharp rise in coverage accommodated by ordering of the adlayer driven by a tendency to minimize the total free energy of the surface;[45−48] the current hump preceding the order−disorder transition has been assigned to the adsorption−desorption of a long-range disordered sulfate adlayer.[46] The presence and sharpness of this peak is strongly tied to the defect density of the surface where, even for evaporated[17] or electrodeposited[26] Pt films on single-crystal substrates, this feature was not observed. CV plots recorded for single crystals miscut to various angles, vicinal surfaces, show a decrease in peak current and eventual disappearance of this peak as the step density is increased and consequently terrace width is decreased.[13,14] We can estimate a minimum average terrace width for the annealed Pt thin films by comparing the CV plot in 0.1 M H_2SO_4 (Figure 1E) to those of a series of miscut Pt(111) single crystals where the fingerprint features of the annealed thin films are closely matched by those of a (13, 13, 12) surface.[13] The butterfly feature between 0.5 and 0.6 V versus RHE in low concentration H_2SO_4 electrolytes (≤0.1 M) disappears for surfaces with an average terrace width below 12 atoms but only under extremely clean conditions.[13,14] It is not uncommon for the butterfly peak to be poorly resolved in H_2SO_4 for surfaces with terrace widths between 20 and 40 atoms.[13] From the electrochemical results, as they represent an average over the entire surface, we can infer a minimum average terrace width of at least 15−20 atoms, confirming a percolating, long-range order of (111) terraces when compared to other CV plots presented in the literature;[13,14] however, locally, as determined by CO_{ad} STM (Figure 1B,C), the annealed Pt thin-film surface contains many areas composed of large, atomically flat terraces with widths greater than 20 nm.

Further insight into the nature of the surface atomic structure of the annealed Pt thin film can be gained through carbon monoxide stripping experiments (Figure 2). It is well-known that CO strongly adsorbs onto Pt, forming an ordered adlayer on wide, atomically flat (111) facets, as shown in Figure 1B,C. The oxidation or stripping of this CO_{ad} layer is very sensitive to surface structure and morphology, being more facile on surfaces with a high density of step edges and defect sites. The overpotential for CO oxidation is lower on highly stepped Pt surfaces because of a combination of higher concentration of oxygenated species as they are preferentially formed at defect sites, aiding the oxidation reaction and a lower CO packing density due to the smaller atomically flat (111) domains.[40,49−51] That being the case, the sharpness and potential of the current peak associated with CO oxidation is strongly tied to the defect density of the Pt surface. For surfaces with higher defect densities, the CO stripping peak will be broad as there is a range of sites with differing coordination and the current peak will occur at a lower potential as CO oxidation is more facile on surfaces with high step and/or defect density. As the surface becomes more ordered, the current peak will sharpen and shift to higher potentials because of the larger proportion of atomically flat (111) domains. Figure 2 shows a significant anodic shift in the peak potential for CO stripping for the annealed Pt thin film in comparison to the as-sputtered Pt thin film as well as a narrowing of the peak. In fact, the potential of the CO stripping peak nearly matches that of a Pt(111) single crystal, which is further indication of the ordered nature and high concentration of large, atomically flat (111) facets present on the annealed Pt thin film.

To generalize the approach presented here, we extend the procedure for ordered thin-film formation to other electrochemically valuable metals. Figure 3 compares CV plots of Au(111) to those of as-sputtered and annealed Au thin films on GC in both $HClO_4$ and H_2SO_4. The current signature in the

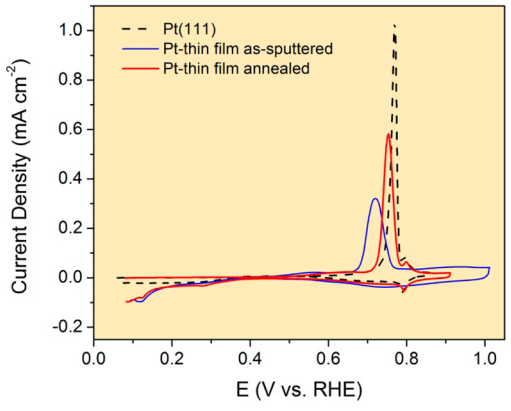

Figure 2. CO stripping curves in 0.1 M $HClO_4$ for Pt(111) (black dashed line), as-sputtered Pt thin film (blue line), and annealed Pt thin film (red line). A CO_{ad} layer was adsorbed onto the Pt electrodes by holding the potential at 0.1 V vs RHE in CO-saturated 0.1 M $HClO_4$ followed by purging of the excess CO through Ar bubbling for 30 min. The CO_{ad} layer was stripped by sweeping the potential anodically at 50 mV s^{-1}.

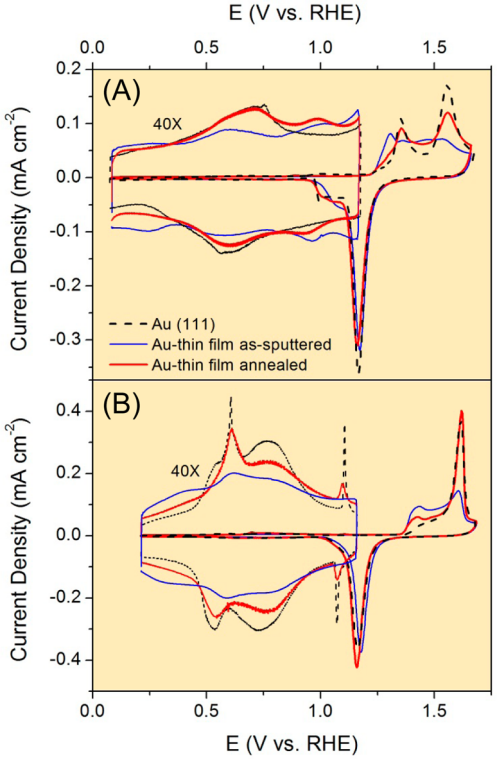

Figure 3. Cyclic voltammograms of Au(111) (black dashed line), as-sputtered Au thin film (blue line) and annealed Au thin film (red line) in room temperature, Ar purged (A) 0.1 M $HClO_4$ and (B) 0.1 M H_2SO_4 recorded with a sweep rate of 50 mV s^{-1}. Low-current region between 0 and 1.2 V vs RHE is magnified by 40 times for clear observation of characteristic current signatures.

dx.doi.org/10.1021/jp4078272 | J. Phys. Chem. C 2013, 117, 23790−23796

low-potential regions is magnified as it shows features that are sensitive to crystallographic orientation. The signature in this low-potential region in $HClO_4$ (Figure 3A) is fairly featureless; however, that in H_2SO_4 (Figure 3B) exhibits features unique to the (111) face. The sharp peak in the anodic scan at ~0.6 V versus RHE has been attributed to the lifting of the reconstruction of the Au(111) surface, moving from a $(\sqrt{3} \times 23)$ to a (1×1) surface.[52−56] The reconstruction is reformed in the cathodic sweep, evidenced by the hump at ~0.55 V versus RHE; the asymmetry of the current feature is due to the slow kinetics of lifting or forming the reconstruction.[57] The peak current of the reconstruction lifting peak on some Au(111) surfaces reported in the literature[53,55] is higher than that shown in Figure 3B. This is due to the fact that the CV plot for Au(111) shown here is recorded after several potential cycles, meaning the peak here may be attributed to the lifting of a potential-induced reconstruction, whereas the higher peak currents seen in the literature are obtained during only the first potential scan after thermal annealing, lifting of thermally induced reconstructions. For the as-sputtered Au film there are no reconstruction peaks; however, for the annealed Au thin film there are clear reconstruction lifting and forming peaks. Moreover, we are able to visualize the $(\sqrt{3} \times 23)$ herringbone reconstruction on the annealed thin film as well as confirm atomically flat terraces with widths of 50−100 nm ubiquitous across the annealed thin film surface through UHV STM (Figure 4B). The herringbone reconstruction is rarely observed

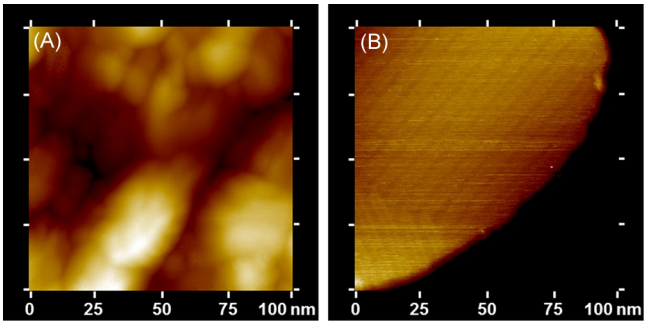

Figure 4. Scanning tunneling microscopy (STM) images recorded in UHV (100 nm ×100 nm), +0.20 V, and 1.0 nA, of (A) as-sputtered Au thin film and (B) an atomically flat Au(111) terrace on an annealed, sputtered Au thin film on a GC disk substrate. The herringbone $(\sqrt{3} \times 23)$ reconstruction is clearly visible, and the terrace width of over 50 nm was routinely found over the entire surface of the annealed, sputtered Au thin films.

with STM on Au thin films as it requires a very clean, ordered surface with wide, atomically flat terraces. In most cases, the herringbone reconstruction was visualized only on evaporated thin films on atomically flat[19,20,58,59] substrates, whereas the films in this study are sputtered deposited onto rough GC substrates, a process that produces a film with smaller grains and a topography with a higher degree of roughness due to the higher rate of deposition and higher kinetic energy of the impinging atoms. The lifting of the reconstruction is accompanied by adsorption of a disordered adlayer of sulfate onto the (111) terrace[54,56] represented by the broad hump between 0.65 and 1 V versus RHE. As the potential is swept anodically, the disordered sulfate adlayer goes through an order−disorder transition to which the sharp, reversible "butterfly" peaks at ~1.1 V versus RHE are attributed.[52−57] The butterfly feature in H_2SO_4 is associated with the long-range order of the surface and disappears for Au(111) surfaces with miscut angles greater than 4° or terrace widths below 3 nm.[15,16,60,61] The presence of this feature, characteristic of surface long-range ordering, for the annealed Au thin film is a direct indication of the (111) structure, smooth morphology, dense nature and overall high quality of the surface.

Expanding the CV potential range into the region of Au oxidation/reduction gives further evidence of the nature of the surface order and structure. In Figure 3A, we see a disappearance of the peak at ~1.3 V versus RHE, which is attributed to AuOH formation at steps and other defect sites[62] after annealing of the thin film, pointing to a smoothening of the surface. The broad current feature between 1.35 and 1.6 V versus RHE transforms into two peaks at ~1.35 and ~1.55 V versus RHE, which is characteristic of Au(111) surfaces and associated with formation of AuOH and AuO layers, respectively, on (111) terraces.[62−64] A decrease in step density upon annealing is also evidenced in H_2SO_4 where a decrease in the height of the feature at ~1.40 V versus RHE and increase in the height and sharpness of the main oxidation peak at ~1.6 V versus RHE follows a smoothening of the surface and a growth in size and population of atomically flat, (111) features.[16]

We have demonstrated the potential viability and general applicability of this approach to other transition metals and even metal oxides through the ordering of two metals, Pt and Au, with differing material properties such as melting point, degree of substrate wetting, and intrinsic stress developed through the sputtering process. Formation of (111)-like features and long-range ordering in thin films is facilitated by the tendency of the topmost atoms to revert to the lowest energy surface in order to minimize overall surface energy. The role of the amorphous substrate is simply to act as a mechanical support without introducing any epitaxial constraint. Surface diffusion is sufficient to drive grain boundary motion and coalescence ultimately leading to grain growth and formation of interconnected long-range ordered (111) facets. We are not reliant on slower bulk diffusion, which allows the use of low annealing temperatures and relatively short annealing times; these (111)-like features are not observed for annealed, bulk polycrystalline Pt electrodes or for Pt thin films sputtered on bulk polycrystalline Pt substrates. From insight generated through this study we see that there exists a threshold in both size and density of atomically well-ordered (111) facets beyond which the polycrystalline thin films exhibit the electrochemical signature of (111) bulk single crystals. The synergistic effect of amorphous substrates and sputtered and annealed well-ordered thin films opens a unique avenue for tailoring functional properties of practical catalysts and precious metal utilization.

4. CONCLUSIONS

The importance of single-crystal electrodes to the field of surface electrochemistry is immeasurable. Valuable insight into the mechanisms of commercially relevant electrochemical processes has been gained over the years through their use. Here we have presented a simple, general procedure to quickly and reproducibly convert sputtered, polycrystalline thin films on inexpensive, amorphous GC substrates into highly ordered, (111)-like thin films exhibiting the characteristic structural and electrochemical features of carefully prepared (111) single-crystal electrodes. Extension of this process to other metal and alloy thin films can facilitate development of a wide range of practical thin-film-based catalysts and help us bridge the gap between bulk and nanoscale surfaces.

dx.doi.org/10.1021/jp4078272 | J. Phys. Chem. C 2013, 117, 23790−23796

AUTHOR INFORMATION

Corresponding Author

*E-mail: vrstamenkovic@anl.gov. Phone: (630) 252-8946.

Notes

The authors declare no competing financial interest.

ACKNOWLEDGMENTS

This work was supported by the U.S. Department of Energy, Office of Science, Office of Basic Energy Sciences, under Contract DE-AC02-06CH11357.

REFERENCES

(1) Markovic, N.; Gasteiger, H.; Ross, P. Oxygen Reduction on Platinum Low-Index Single-Crystal Surfaces in Sulfuric Acid Solution: Rotating Ring−Pt(*hkl*) Disk Studies. *J. Phys. Chem.* **1995**, *99*, 3411−3415.

(2) Markovic, N.; Schmidt, T.; Stamenkovic, V.; Ross, P. Oxygen Reduction Reaction on Pt and Pt Bimetallic Surfaces: A Selective Review. *Fuel Cells* **2001**, *1*, 105−116.

(3) Markovic, N.; Adzic, R.; Cahan, B.; Yeager, E. Structural Effect in Electrocatalysis: Oxygen Reduction on Platinum Low Index Single-Crystal Surfaces in Perchloric Acid Solutions. *J. Electroanal. Chem.* **1994**, *377*, 249−259.

(4) Macia, M.; Herrero, E.; Feliu, J. On the Kinetics of Oxygen Reduction on Platinum Stepped Surfaces in Acidic Media. *J. Electroanal. Chem.* **2004**, *564*, 141−150.

(5) van der Vliet, D.; Wang, C.; Tripkovic, D.; Strmcnik, D.; Zhang, X.; Debe, M.; Atanasoski, R.; Markovic, N.; Stamenkovic, V. Mesostructured Thin Films as Electrocatalysts with Tunable Composition and Surface Morphology. *Nat. Mater.* **2012**, *11*, 1051−1058.

(6) Markovic, N.; Gasteiger, H.; Ross, P. Kinetics of Oxygen Reduction on Pt(*hlk*) Electrodes: Implications for the Crystallite Size Effect with Supported Pt Electrocatalysts. *J. Electrochem. Soc.* **1997**, *144*, 1591−1597.

(7) Greely, J.; Rossmeisl, J.; Hellman, A.; Norskov, J. Theoretical Trends in Particle Size Effects for the Oxygen Reduction Reaction. *Z. Phys. Chem.* **2007**, *221*, 1209−1220.

(8) Climent, V.; Feliu, J. Thirty Years of Platinum Single Crystal Electrochemistry. *J. Solid State Electrochem.* **2011**, *15*, 1297−1315.

(9) Stamenkovic, V.; Fowler, B.; Mun, B.; Wang, G.; Ross, P.; Lucas, C.; Markovic, N. Imporved Oxygen Reduction Activity on $Pt_3Ni(111)$ via Increased Site Availability. *Science* **2007**, *315*, 493−497.

(10) Clavilier, J.; Faure, R.; Guinet, G.; Durand, R. Preparation of Monocrystalline Pt Microelectrodes and Electrochemical Study of the Plane Surfaces Cut in the Direction of the {111} and {110} Planes. *J. Electroanal. Chem.* **1979**, *107*, 205−209.

(11) Clavilier, J.; Armand, D.; Wu, B. Electrochemical Study of the Initial Surface Condition of Platinum Surfaces with (100) and (111) Orientations. *J. Electroanal. Chem. Interfacial Electrochem.* **1982**, *135*, 159−166.

(12) Clavilier, J. The Role of Anion on the Electrochemical Behavior of a {111} Platinum Surface; An Unusual Splitting of the Voltammogram in the Hydrogen Region. *J. Electroanal. Chem.* **1979**, *107*, 211.

(13) Clavilier, J.; El Achi, K.; Rodes, A. In Situ Probing of Step and Terrace Sites on Pt(S)-[*n*(111) × (111)] Electrodes. *Chem. Phys.* **1990**, *141*, 1−14.

(14) Furuya, N.; Koide, S. Hydrogen Adsorption on Plaitnum Single-Crystal Surfaces. *Surf. Sci.* **1989**, *220*, 18−28.

(15) Wandlowski, T.; Ataka, K.; Pronkin, S.; Diesing, D. Surface Enhanced Infrared Spectroscopy—Au(111−20 nm)/Sulfuric Acid—New Aspects and Challenges. *Electrochim. Acta* **2004**, *49*, 1233−1247.

(16) Schneeweiss, M.; Kolb, D.; Liu, D.; Mandler, D. Anodic Oxidation of Au(111). *Can. J. Chem.* **1997**, *75*, 1703−1709.

(17) Braunschweig, B.; Mitin, A.; Daum, W. Pt(111) Thin-Layer Elecrodes on α-$Al_2O_3(0001)$: Morphology and Atomic Structure. *Surf. Sci.* **2011**, *605*, 1082−1089.

(18) Golan, Y.; Margulis, L.; Rubinstein, I. Vacumm-Deposited Gold Films, I. Factors Affecting the Film Morphology. *Surf. Sci.* **1992**, *264*, 312−326.

(19) Spiridis, N.; Kisielewski, M.; Maziewski, A.; Slezak, T.; Cyganik, P.; Korecki, J. Correlation of Morphology and Magnetic Properties in Ultrathin Epitaxial Co Films on Au(111). *Surf. Sci.* **2002**, *507−510*, 546−552.

(20) Broukhin, S.; Saguy, C.; Koifman, M.; Pokroy, B. Self-Ordered Vicinal-Surface-Like Nanosteps at the Thin Metal-Film/Substrate Interface. *J. Phys. Chem. C* **2012**, *116*, 12149−12155.

(21) Trevor, D.; Chidsey, C.; Loiacono, D. In Situ Scanning-Tunneling-Microscope Observation of Roughening, Annealing, and Dissolution of Gold (111) in an Electrochemical Cell. *Phys. Rev. Lett.* **1989**, *62*, 929−932.

(22) Scavia, G.; Agostinelli, E.; Laureti, S.; Varvaro, G.; Paci, B.; Benerosi, A.; Albertini, V.; Kaciulis, S.; Mezzi, A. Evolution of the Pt Layer Deposited on MgO(001) by Pulsed Laser Deposition as a Function of the Deposition Parameters: A Scanning Tunneling Microscopy and Energy Dispersive X-ray Diffractometry/Reflectometry Study. *J. Phys. Chem. B* **2006**, *110*, 5529−5536.

(23) Debe, M. Electrocatalyst Approaches and Challenges for Automotive Fuel Cells. *Nature* **2012**, *486*, 43−51.

(24) Yamada, Y.; Miyamoto, K.; Hayashi, T.; Iijima, Y.; Todoroki, N.; Wadayama, T. Oxygen Reduction Reaction Activities of Pt-Enriched Co/Pt(111), and Co/Pt(110) Model Catalyst Surfaces Prepared by Molecular Beam Epitaxy. *Surf. Sci.* **2013**, *607*, 54−60.

(25) Liu, Y.; Gokcen, D.; Bertocci, U.; Moffat, T. Self-Terminating Growth of Platinum Films by Electrochemical Depsition. *Science* **2012**, *338*, 1327−1330.

(26) Uosaki, K.; Ye, S.; Naohara, H.; Oda, Y.; Haba, T.; Kondo, T. Electrochemical Epitaxial Growth of a Pt(111) Phase on a Au(111) Electrode. *J. Phys. Chem. B* **1997**, *101*, 7566−7572.

(27) Berna, A.; Delgado, J.; Orts, J.; Rodes, A.; Feliu, J. In-Situ Infrared Study of the Adsorption and Oxidation of Oxalic Acid at Single-Crystal and Thin-Film Gold Electrodes: A Combined External Reflection Infrared and ATR-SEIRAS Approach. *Langmuir* **2006**, *22*, 7192−7202.

(28) Maljusch, A.; Henry, J.; Schuhmann, W.; Bondarenko, A. A Quick Method for the Preparation of Pt(111)-like Thin Films. *Electrochem. Commun.* **2012**, *16*, 88−91.

(29) Henry, J.; Maljusch, A.; Huang, M.; Schuhmann, W.; Bondarenko, A. Thin-Film Cu-Pt(111) Near-Surface Alloys: Active Electrocatalysts for the Oxygen Reduction Reaction. *ACS Catalysis* **2012**, *2*, 1457−1460.

(30) Kawamura, M.; Mashima, T.; Abe, Y.; Sasaki, K. Formation of Ultra-Thin Continuous Pt and Al Films by RF Sputtering. *Thin Solid Films* **2000**, *377−378*, 537−542.

(31) Slavcheva, E.; Ganske, G.; Topalov, G.; Mokwa, W.; Schnakenberg, U. Effect of Sputtering Parameters on Surface Morphology and Catalytic Efficiency of Thin Platinum Films. *Appl. Surf. Sci.* **2009**, *255*, 6479−6486.

(32) Thornton, J.; Hoffman, D. The Influence of Discharge Current on the Intrinsic Stress in Mo Films Deposited Using Cylindrical and Planar Magnetron Sputtering Sources. *J. Vac. Sci. Technol., A* **1985**, *3*, 576−579.

(33) Cuthrell, R.; Mattox, D.; Peeples, C.; Dreike, P.; Lamppa, K. Residual Stress Anisotropy, Stress Control, and Resistivity in Post Cathode Magnetron Sputter Deposited Molybdenum Films. *J. Vac. Sci. Technol., A* **1988**, *6*, 2914−2920.

(34) Mattox, D. Particle Bombardment Effects on Thin Film Deposition: A Review. *J. Vac. Sci. Technol., A* **1989**, *7*, 1105−1114.

(35) Tersoff, J.; LeGoues, F. Competing Relaxation Mechanisms in Strained Layers. *Phys. Rev. Lett.* **1994**, *72*, 3570−3573.

(36) Galinski, H.; Ryll, T.; Schlagenhauf, L.; Gauckler, L. Hillock Formation of Pt Thin Films on Single-Crystal Yttria-Stabilized Zirconia. *Phys. Rev. B* **2012**, *85*, 125408.

(37) Pennebaker, W. Hillock Growth and Stress Relief in Sputtered Au Films. *J. Appl. Phys.* **1969**, *40*, 394−400.
(38) Rost, M.; Quist, D.; Frenken, J. Grains, Growth and Grooving. *Phys. Rev. Lett.* **2003**, *91*, 026101.
(39) Hwang, S.-J.; Jee, J.-H.; Jeong, C.-O.; Joo, Y.-C. Effect of Film Thickness and Annealing Temperature on Hillock Distributions in Pure Al Films. *Scr. Mat.* **2007**, *56*, 17−20.
(40) Strmcnik, D.; Tripkovic, D.; van der Vliet, D.; Chang, K.; Komanicky, V.; You, H.; Karapetrov, G.; Greeley, J.; Stamenkovic, V.; Markovic, N. Unique Activity of Platinum Adislands in the CO Electrooxidation Reaction. *J. Am. Chem. Soc.* **2008**, *130*, 15332−15339.
(41) Bondarenko, A.; Stephens, I.; Hansen, H.; Perez-Alonso, F.; Tripovic, V.; Johansson, T.; Rossmeisl, J.; Norskov, J.; Chorkendorff, I. The Pt(111)/Electrolyte Interface under Oxygen Reduction Reaction Conditions: An Electrochemical Impedance Spectroscopy Study. *Langmuir* **2011**, *27*, 2058−2066.
(42) Berna, A.; Climent, V.; Feliu, J. New Understanding of the Nature of OH Adsorption on Pt(111) Electrodes. *Electrochem. Commun.* **2007**, *9*, 2789−2794.
(43) Herrero, E.; Feliu, J.; Wieckowski, A.; Clavilier, J. The Unusual Adsorption States of Pt(111) Electrodes Studied by an Iodine Displacement Method: Comparison with Au(111) Electrodes. *Surf. Sci.* **1995**, *325*, 131−138.
(44) Markovic, N.; Schmidt, T.; Grgur, B.; Gasteiger, H.; Behm, R.; Ross, P. Effect of Temperature on Surface Processes at the Pt(111)−Liquid Interface: Hydrogen Adsorption, Oxide Formation, and CO Oxidation. *J. Phys. Chem. B* **1999**, *103*, 8568−8577.
(45) Garcia-Araez, N.; Climent, V.; Rodriguez, P.; Feliu, J. Thermodynamic Analysis of (Bi)sulfate Adsorption on a Pt(111) Electrode as a Function of pH. *Electrochim. Acta* **2008**, *53*, 6793−6806.
(46) Koper, M.; Lukkien, J. Modeling the Butterfly: The Voltammetry of $(\sqrt{3} \times \sqrt{3})$R30° and p(2 × 2) Overlayers on (111) Electrodes. *J. Electroanal. Chem.* **2000**, *485*, 161−165.
(47) Braunschweig, B.; Daum, W. Superstructures and Order-Disorder Transition of Sulfate Adlayers on Pt(111) in Sulfuric Acid Solution. *Langmuir* **2009**, *25*, 11112−11120.
(48) Funtikov, A.; Stimming, U.; Vogel, R. Anion Adsorption from Sulfuric Acid Solution on Pt(111) Single Crystal Electrodes. *J. Electroanal. Chem.* **1997**, *428*, 147−153.
(49) Lebedeva, N.; Koper, M.; Herrero, E.; Feliu, J.; van Santen, R. Cooxidation on Stepped Pt[n(111) × 111)] Electrodes. *J. Electroanal. Chem.* **2000**, *487*, 37−44.
(50) Lebedeva, N.; Rodea, A.; Feliu, J.; Koper, M.; van Santen, R. Role of Crystalline Defects in Electrocatalysis: CO Adsorption and Oxidation on Stepped Platinum Electrodes As Studied by in situ Infrared Spectroscopy. *J. Phys. Chem. B* **2002**, *106*, 9863−9872.
(51) Lebedeva, N.; Koper, M.; Feliu, J.; van Santen, R. Mechanism and Kinetics of the Electrochemical CO Adlayer Oxidation on Pt(111). *J. Electroanal. Chem.* **2002**, *524*−*525*, 242−251.
(52) Schneeweiss, M.; Kolb, D. Oxide Formation on Au(111). *Solid State Ionics* **1997**, *94*, 171−179.
(53) Sato, K.; Yoshimoto, S.; Inukai, J.; Itaya, K. Effect of Sulfuric Acid Concentration on the Structure of Sulfate Adlayer on Au(111) Electrode. *Electrochem. Commun.* **2006**, *8*, 725−730.
(54) Magnussen, O.; Hagebock, J.; Hotlos, J.; Behm, R. *In situ* Scanning Tunneling Microscopy Observations of a Disorder−Order Phase Transition in Hydrogensulfate Adlayers on Au(111). *Faraday Discuss.* **1992**, *94*, 329−338.
(55) Silva, F.; Martins, A. Surface Reconstruction of Gold Single Crystals: Evidence of the Effect of Adsorbed Anions and Influence of Steps and Terraces. *Electrochim. Acta* **1998**, *44*, 919−929.
(56) Kondo, T.; Morita, J.; Hanaoka, K.; Takakusagi, S.; Tamura, K.; Takahasi, M.; Mizuki, J.; Uosaki, K. Structure of Au(111) and Au(100) Single-Crystal Electrode Surfaces at Various Potentials in Sulfuric Acid Solution Determined by In Situ Surface X-ray Scattering. *J. Phys. Chem. C* **2007**, *111*, 13197−13204.
(57) Shi, Z.; Lipkowski, J.; Mirwald, S.; Pettinger, B. Electrochemical and Second Harmonic Generation Study of SO_4^{2-} Adsorption at the Au(111) Electrode. *J. Electroanal. Chem.* **1995**, *396*, 115−124.
(58) Kowalczyk, P.; Kozlowski, W.; Klusek, Z.; Olejniczak, W.; Datta, P. STM Studies of the Reconstructed Au(111) Thin-Film at Elevated Temperatures. *Appl. Surf. Sci.* **2007**, *235*, 4715−4720.
(59) Lussem, B.; Karthauser, S.; Haselier, H.; Waser, R. The Origin of Faceting of Ultraflat Gold Films Epitaxially Grown on Mica. *Appl. Surf. Sci.* **2005**, *249*, 197−202.
(60) Cuesta, A.; Kleinert, M.; Kolb, D. The Adsorption of Sulfate and Phosphate on Au(111) and Au(100) Electrodes: An in-situ STM Study. *Phys. Chem. Chem. Phys.* **2000**, *2*, 5684−5690.
(61) Holzle, M.; Zwing, V.; Kolb, D. The Influence of Steps on the Deposition of Cu onto Au(111). *Electrochim. Acta* **1995**, *40*, 1237−1247.
(62) Vitus, C.; Davenport, A. In Situ Scanning Tunneling Microscopy Studies of the Formation and Reduction of a Gold Oxide Monolayer on Au(111). *J. Electrochem. Soc.* **1994**, *141*, 1291−1298.
(63) Hondo, H.; Sugawara, S.; Itaya, K. Detailed in Situ Scanning Tunneling Microscopy of Single Crystal Planes of Gold(111) in Aqueous Solution. *Anal. Chem.* **1990**, *62*, 2424−2429.
(64) Hamelin, A. Cyclic Voltammetry at Gold Single-Crystal Surfaces. Part 1. Behavior at Low-Index Faces. *J. Electroanal. Chem.* **1996**, *407*, 1−11.